Journal of Power Sources 561 (2023) 232749

Contents lists available at ScienceDirect

Journal of Power Sources

journal homepage: www.elsevier.com/locate/jpowsour

Uncertainty analysis of selected standard methods in battery measurement technology

Bernhard Schweighofer *, Daniel Schürholz, Markus Neumayer, Hannes Wegleiter

Christian Doppler Laboratory for Measurement Systems for Harsh Operating Conditions, Institute of Electrical Measurement and Sensor Systems, Graz University of Technology, Inffeldgasse 33, 8010 Graz, Austria

HIGHLIGHTS

- Ratiometric quantities, e.g. ΔC or CE, reach uncertainties in the low ppm range.
- Non-ratiometric quantities, e.g. capacitance, are much worse at several 100 ppm.
- The value-to-value jitter is very low, ranging from a few to a few tens of ppm.
- For low uncertainty, a highly stable temperature control (few mK) is necessary.

ARTICLE INFO

Keywords:
High-precision battery measurements
Uncertainty analysis
Coulombic efficiency
Differential capacity analysis

ABSTRACT

Measuring the state of batteries and their change over time is essential during research and development. A number of standard test methods are available to determine specific cell parameters, such as capacitance, internal resistance, coulombic efficiency, etc. Although these methods have been in use for a long time, a thorough analysis of the uncertainties associated with them – especially when using high-precision measuring equipment – is still lacking.

Therefore, a primary goal of this work is to close this gap. For each method, the results of the uncertainty analysis are divided into a variable part (noise, jitter) and a constant part (absolute accuracy). In addition, the theoretical analysis is accompanied by practical measurement results from a high-precision measurement hardware, demonstrating what is currently possible with state-of-the-art equipment.

The constant part of the uncertainty is mainly limited by the used calibration equipment. For the variable part of uncertainty, the situation is somewhat more varied. Using a battery temperature control with a variability of only ±0.1 °C, capacity, capacity change and coulombic efficiency still show a strong influence on the prevailing small temperature variations. For the voltage analysis methods (differential capacity and voltage analysis) the predominate factor is voltage noise and drift.

1. Introduction

In battery research and development, it is essential to measure the state of a battery and its change over time or cycles. There are many test procedures to electrically measure the condition of a battery [1,2]. One of the most commonly used test methods is to measure the capacity of the battery. In addition, continuous charge/discharge cycles can then be used to measure capacity degradation over time, allowing predictions of achievable (cycle-) life. A slightly modified variant of this test method is shown in Fig. 1, which is applicable to all types of lithium-ion cells, regardless of their chemistry. Compared to a normal cycling, the constant voltage phase with declining current amplitude at the end of charge – to reach the 'true' fully-charged state – is missing. Due to this change, there remains only a single constant current amplitude – with different signs for charge and discharge – during the entire time. This modification eases the development of high-precision measuring equipment.

With such equipment, in addition to the capacity measurement, a variety of further analysis methods can be applied to the same measurement data, e.g. differential capacity and voltage analysis, determination of the Coulombic efficiency, and calculation of the internal resistance of the battery. All these methods can be considered as state of the art. But a thorough analysis or consideration of the associated uncertainties is often neglected, respectively, there is almost no literature on this

* Corresponding author.
E-mail address: bernhard.schweighofer@tugraz.at (B. Schweighofer).

https://doi.org/10.1016/j.jpowsour.2023.232749
Received 7 November 2022; Received in revised form 25 January 2023; Accepted 27 January 2023
Available online 2 February 2023

Nomenclature

Abbreviations

CE	Coulombic efficiency
DCA	Differential capacity analysis
DVA	Differential voltage analysis
GUM	Guide to the expression of uncertainty in measurement
OCV	Open circuit voltage
SOC	State of charge

Greek Symbols

Δx	Change of quantity x
η	Efficiency
ϑ	Temperature, °C

Roman Symbols

CE	CE-value
DCA	DCA-value, As/V
DVA	DVA-value, V/As
e	Relative error
E	Absolute error
s	Sensitivity
f	Frequency, Hz
I	Current, A
M	Number of samples
Q	Charge, As
R	Resistance, Ω
t	Time, s
T	Time duration, s
TCR	Temperature coefficient of resistance, Ω/K
TCV	Temperature coefficient of voltage, V/K
u	Uncertainty
V	Voltage, V
V_{low}, V_{high}	Lower and upper voltage switchpoint, V
$\bar{x}$	Mean value of x

Subscript

avg	Average
c	Calibration
C	Charge
const	Constant (part)
DC	Discharge
meas	Measurement
m or n	Cycle number (index)
N	Number of cycles (distance)
ref	Reference (cycle)
r	Range
ϑ	Temperature
td	Time-drift
var	Variable (part)

subject. The aim of this publication is to close this gap and to give the user a deep insight into the underlying relationships.

In order to be able to give not only a theoretical analysis, but also practice relevant numerical values, a commercial Li-Ion cell is measured with a high precision measurement system. In particular, this also serves to show the extent to which changes in the measurement results are actually caused by the cell under test, as desired, or are possibly influenced by the measurement system or ambient conditions.

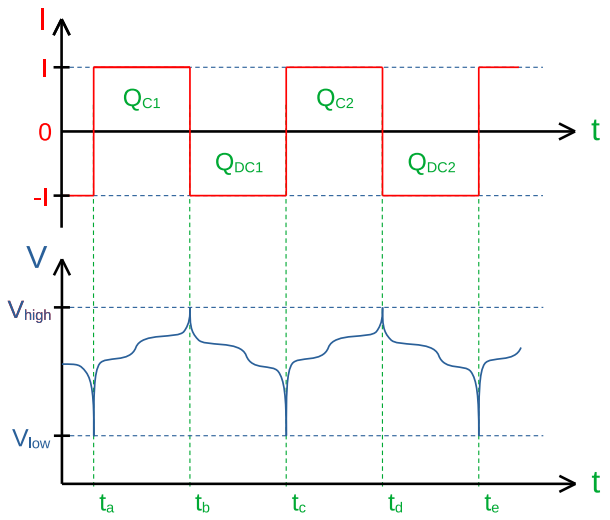

Fig. 1. Schematic representation of battery current I and voltage V during constant current cycling.

In Section 2, the individual analysis methods are briefly explained. Afterwards, in Section 3, the characteristics of the used test equipment and battery are shown, followed by Section 4, with a detailed analysis of the sources of uncertainty and their effects. Finally, in Section 5, the paper concludes with a brief summary of the lessons learned and pitfalls that need to be considered.

2. Data analysis methods

In the following, each of the methods mentioned in the introduction are explained in more detail. Additionally, in order to be able to give more than just a theoretical sketch, a commercially available LG INR18650 MJ1 lithium ion battery with 3.5 Ah capacity from LG Chem is measured to create corresponding diagrams. The measurement conditions are a test current of $I = 0.875$ A, a constant air temperature of $\vartheta_{air} = 40$ °C, and a voltage range of $V_{low} = 2.5$ V to $V_{high} = 4.2$ V.

2.1. Capacity

The most basic analysis is to evaluate the discharge capacity $Q_{discharge}$

$$Q_{discharge} = \int_{t_0}^{t_1} I \, dt \tag{1}$$

with current amplitude I and time t between the start of discharge t_0 and its end t_1 (Fig. 2a). For example the first discharge capacity Q_{DC1} in Fig. 1 can be calculated as

$$Q_{DC1} = \int_{t_b}^{t_c} I \, dt \tag{2}$$

This is also one of the most important parameters of a battery, since it is directly related to the amount of energy that can be extracted [3].

Since the final constant voltage phase is missing during charging, this calculated value is not directly comparable with the value from the data sheet, it will be somewhat lower. It would therefore be more correct to speak of a 'pseudo-capacitance measurement', but in the further text this subtlety is neglected and we continue to speak of 'capacitance measurement'.

In most cases, it is not the capacity itself that is of interest, but the change in capacity over time. Based on an extrapolation of the curve towards higher cycle numbers, an attempt is then made to derive

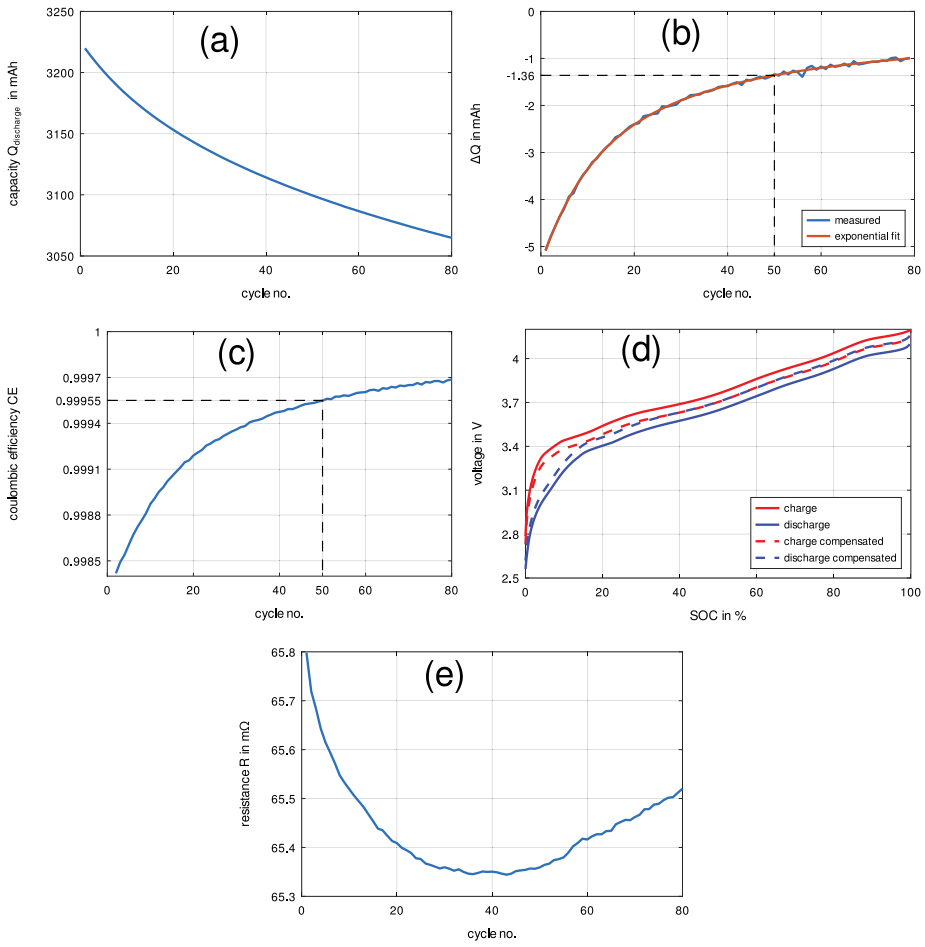

Fig. 2. (a) Battery discharge capacity $Q_{\text{discharge}}$ over cycles of the LG MJ1 cell at 40 °C. (b) Capacity change per cycle ΔQ. (c) Coulombic efficiency CE. (d) Battery voltage V as a function of state of charge SOC. The 'compensated' curves have been obtained by shifting these curves by the voltage drop at the internal resistance measured at $SOC \approx 50\%$ (see also Fig. 4b). (e) Internal resistance R.

the available service life. Usually 80 % of the original capacity (20 % degradation) is assumed as the end-of-life limit [4,5]. For the necessary approximation of the curve, it is best to consider the corresponding decrease of capacity per cycle (Fig. 2b)

$$\Delta Q_{\text{n}} = Q_{\text{n+1}} - Q_{\text{n}} \tag{3}$$

with index n going from 1 to the number of measured cycles minus one. This curve can then usually be approximated by a simple linear or, in this case, exponential fit

$$\Delta Q_{\text{approx}} = \hat{Q}_2 \cdot (1 - \text{e}^{-\text{cycle no.}/\tau_2}) + \hat{Q}_1 \cdot (1 - \text{e}^{-\text{cycle no.}/\tau_1}) + Q_0 \tag{4}$$

with τ_1, τ_2, Q_0, $\hat{Q}_1$ and $\hat{Q}_2$ parameters for the fit. By integrating this curve over the number of cycles until the desired amount of damage is reached, the expected cycle life can be calculated. For the example shown, almost 800 cycles are required until 20 % deterioration is reached.

2.2. Coulombic efficiency

Calculating the ratio between discharge capacity and preceding charge capacity (e.g. Q_{DC1} and Q_{C1} in Fig. 1), one obtains the 'Coulombic efficiency' (Fig. 2c) [6–9]

$$CE = \frac{Q_{\text{discharge}}}{Q_{\text{charge}}} \tag{5}$$

An ideal (lossless) battery would have a Coulombic efficiency of 1, but parasitic reactions take place that consume charge, e.g. self-discharge, causing the discharge capacity to decrease relative to the charge capacity and the Coulombic efficiency becomes lower than 1. This also shows the utility of this parameter — the characterization of (life-reducing) parasitic reactions [10,11].

Comparing the decline of capacity ('damage' of the battery) in Fig. 2b for cycle no. 50 (1.36 mAh/cycle, corresponding 439 ppm/cycle if referred to the measured capacity of 3100 mAh for the 50th cycle) with the Coulombic efficiency in Fig. 2c of 0.99955 (450 ppm below 1), almost no difference can be observed. This indicates that most of the parasitic reactions actually have a damaging effect on the battery and only a small amount is non-damaging, e.g. leakage currents [12].

2.3. Internal resistance

In Fig. 2d, the battery voltage is plotted versus state of charge SOC instead of time. A clear difference can be seen between charge and discharge curves. With the help of the equivalent circuit of a battery in Fig. 3, this difference can be explained as the effect of the voltage drop at the internal impedance [13]. For steady state, the complex RLC-network can be reduced to a single resistor R, which greatly eases further analysis. Its value is another important parameter indicating the performance (power rating) of a battery.

Assuming that the internal resistance R is the same during charge and discharge, which corresponds quite well to reality, it can be calculated as

$$R(SOC) = \frac{V_{\text{charge}}(SOC) - V_{\text{discharge}}(SOC)}{2 \cdot I} \tag{6}$$

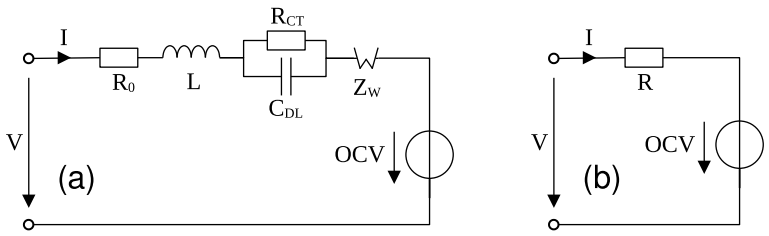

Fig. 3. (a) Detailed equivalent circuit diagram of a battery with internal resistance R_0, inductance L, charge transfer resistance R_{CT}, double layer capacity C_{DL}, Warburg impedance Z_W and open circuit voltage OCV [14–16]. (b) Simplified version for steady state, the RLC-network has been replaced by a single resistor R.

with current amplitude I and voltage during charge $V_{charge}(SOC)$ and discharge $V_{discharge}(SOC)$ at state of charge SOC respectively.

Since it takes some time to reach steady state after switching the current direction, the begin of charge and discharge (high and low state of charge) have to be removed from the calculation. In addition, usually only a state of charge independent (average) resistance is of interest. For example, in the result shown in Fig. 2e, only the average resistance $\bar{R}$, for the state of charge range from $r = 45 \ldots 55\%$, has been calculated:

$$\bar{R} = \frac{\overline{V}_{\text{charge}}(r) - \overline{V}_{\text{discharge}}(r)}{2 \cdot I} \tag{7}$$

Like with the capacity analysis, the change over time indicates the aging of the battery.

2.4. Differential capacity analysis

Differential capacity analysis (DCA) evaluates the inverse slope of the voltage curve (Fig. 4a):

$$DCA = \frac{\mathrm{d}Q}{\mathrm{d}V} \tag{8}$$

The flatter the measured voltage of the cell, e.g. at voltage-plateaus, the higher the corresponding peak values in the DCA curve. DCA is a method that allows for a deeper insight into the electrochemical processes during charging and discharging. The peaks typically indicate the intercalation of ions into or out of an electrode at a given cell voltage, whereas the height and width of these peaks provides additional information about this process [17].

Due to the voltage hysteresis between charge and discharge (see Fig. 2d), the corresponding peaks are shifted to the left and right, respectively (Fig. 4a). To compensate for this effect, one can use a modified voltage curve, where the curves have been shifted by this voltage drop ('compensated curves' in Fig. 2d), resulting in an adjusted plot shown in Fig. 4b.

As the battery ages, the peaks in the DCA-curve shift in position and change their amplitude. To better visualize this, the difference between two DCA-curves is used [18,19]

$$\Delta DCA_{\text{ref}} = DCA_{\text{ref+1}} - DCA_{\text{ref}} \tag{9}$$

Due to the small changes inside the battery, the visible difference between current and previous cycle is often too small — the result is dominated by measurement noise. Therefore, depending on the quality of the measurement equipment, this difference has to be increased (typically to about $N = 5$ to 20 cycles)

$$\Delta DCA_{\text{ref,N}} = \frac{DCA_{\text{ref+N}} - DCA_{\text{ref}}}{N} \tag{10}$$

Fig. 4c shows the ΔDCA for cycle $ref = 2$ and a distance of $N = 5$.

2.5. Differential voltage analysis

The differential voltage analysis (DVA) value is calculated as reciprocal of the DCA-value (Fig. 4d):

$$DVA = \frac{1}{DCA} = \frac{\mathrm{d}V}{\mathrm{d}Q} \tag{11}$$

In contrast to the DCA, which has its peaks at the plateaus of the voltage curve, the DVA visualizes steep slopes which typically occur at the begin and end of charge/discharge. DVA can therefore be regarded as the counterpart to the DCA [20,21].

Like with DCA, the age-induced changes inside the cell can be visualized by plotting the difference between two DVA values accordingly (Fig. 4e). Here, too, the difference between the two cycles N must usually be selected to be greater than 1, to achieve a meaningful result with low noise

$$\Delta DVA_{\text{ref,N}} = \frac{DVA_{\text{ref+N}} - DVA_{\text{ref}}}{N} \tag{12}$$

3. Uncertainty analysis — Prerequisites

Only by specifying an associated uncertainty does a measurement unfold its full substance. Given the setup as shown in Fig. 5, there are two sources of uncertainty. On the one hand, the test equipment — uncertainties related with the imprinted battery current and the measurement of voltage, current and time. On the other hand, the battery itself contains some 'hidden' sources affecting the overall uncertainty.

Thus, before presenting the uncertainty analysis for the given data analysis methods in Section 4, the corresponding uncertainties of the test equipment and battery are explained first. For the uncertainty analysis, the framework described in the 'Guide to the Expression of Uncertainty in Measurement' (GUM) is used [22,23]. Again, the data of the measurement system and the LG MJ1 battery are used to have some practical numerical samples for each calculation.

3.1. Test equipment

Within the scope of this work, we deal with high-precision measurements on batteries. It is therefore necessary to take appropriate care when stating uncertainties. To better account for the influencing factors, the uncertainty is decomposed into individual contributions. The calibration uncertainty u_c is the initial uncertainty that results from calibrating the test equipment. Time after calibration and temperature changes will cause the instrument to drift, and are described by the cross-sensitivities for time-drift s_{td} and temperature s_ϑ. Finally, even if the same value is measured several times in succession, the displayed values will fluctuate slightly, which is covered by the noise uncertainty u_n. Time-drift and temperature induced uncertainties depend on time after calibration T_c, time duration of the measurement itself T_{meas}, and temperature fluctuation u_ϑ. Additionally, all values are either given as absolute values, relative to the full-scale range, or relative to the actual measured value — which has to be considered correspondingly. For example, assuming all values have been given as absolute values, the total uncertainty u_{total} can then be calculated as

$$u_{\text{total}} = \sqrt{u_c^2 + [s_{td} \cdot (T_c + T_{meas})]^2 + (s_\vartheta \cdot u_\vartheta)^2 + u_n^2} \tag{13}$$

The term $(T_c + T_{meas})^2$ can be split into

$$(T_c + T_{meas})^2 = T_c^2 + 2 \cdot T_c \cdot T_{meas} + T_{meas}^2 \tag{14}$$

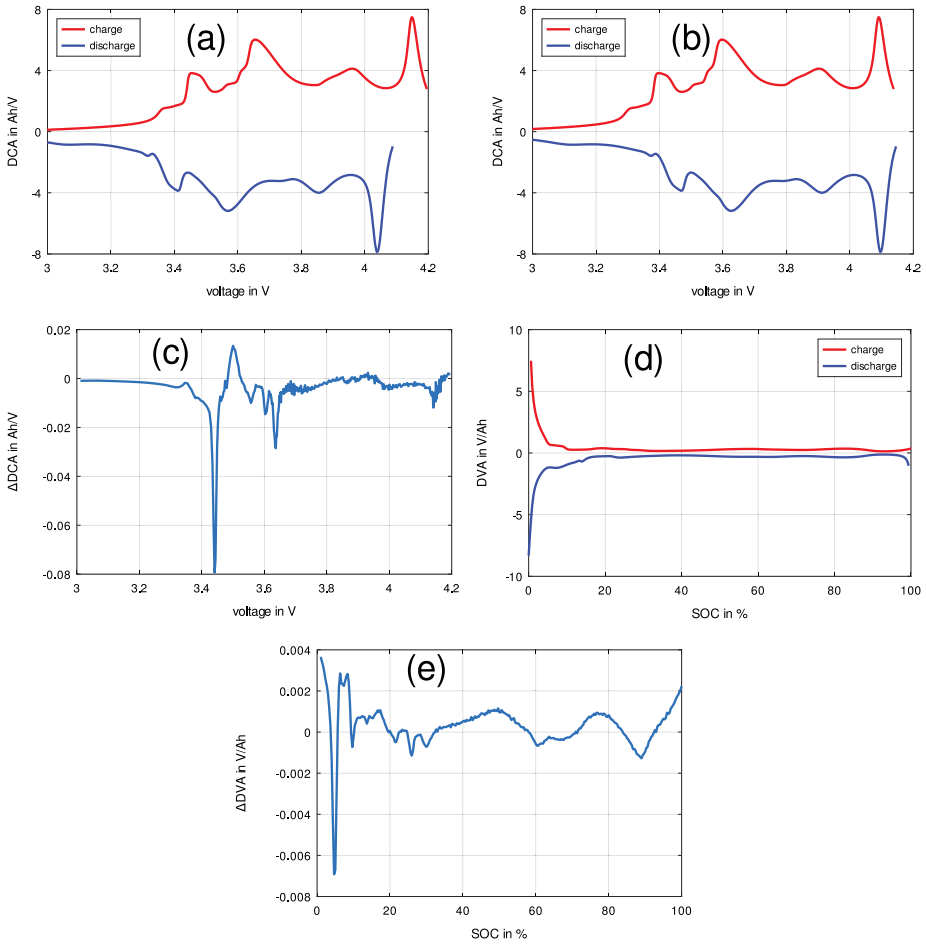

Fig. 4. (a) Differential Capacity Analysis DCA of the LG MJ1 cell at 40 °C for the second charge/discharge cycle. (b) DCA with compensated (shifted) voltage-axis (see also Fig. 2d). (c) Delta differential capacity analysis $\Delta DCA_{2,5}$ ($ref = 2$, $N = 5$). (d) Differential voltage analysis DVA. (e) Delta differential voltage analysis $\Delta DVA_{2,5}$.

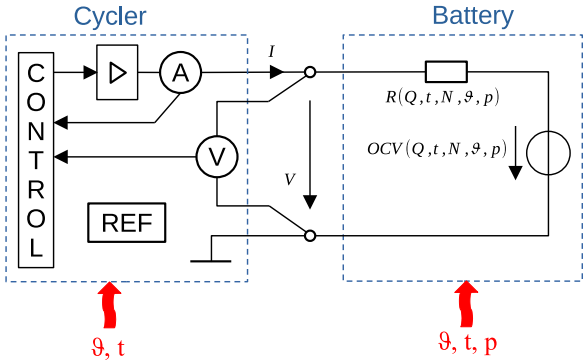

Fig. 5. Measurement setup for battery cycling. The current is kept constant by means of a software control loop. The main external interfering factors for the cycler and the battery are given underneath (time t, temperature ϑ, pressure p). The parameters of the (simplified) battery model – resistance R and open circuit voltage OCV – are additionally dependent on the state-of-charge (charge state Q) and cycle number N.

and under the assumption that $T_c \gg T_{meas}$, the first two terms can be approximated by

$$T_c^2 + 2 \cdot T_c \cdot T_{meas} \approx T_c^2 \tag{15}$$

For the further calculation it is then useful to divide the total uncertainty u_{total} into a part which is constant during the measurement u_{const} and a variable part u_{var} which summarizes random influences:

$$u_{const} \approx \sqrt{u_c^2 + (s_{td} \cdot T_c)^2} \tag{16}$$

$$u_{var} \approx \sqrt{(s_{td} \cdot T_{meas})^2 + (s_\vartheta \cdot u_\vartheta)^2 + u_n^2} \tag{17}$$

$$u_{total} = \sqrt{u_{const}^2 + u_{var}^2} \tag{18}$$

During the initial calibration, the measurands are adjusted to their calibration targets. But a residual (constant) error between measurement and 'true value' remains. This is typically considered by a corresponding calibration uncertainty u_c. But it can also be directly expressed by using the (unknown) relative error e_x,[1] and by further substituting each measurand X by $X \cdot (1 + e_x)$. Especially in cases, where multiple measurements are compared against each other, e.g. capacity decrease over time or Coulombic efficiency, this eases the consideration of constant and variable influences on the final calculation result, as will be shown later. Still, when calculating the final (total) uncertainty the e_x terms are again substituted by its corresponding uncertainties.

There are different strategies for determining the uncertainties for the different measurands (voltage, current, and time). For the time

[1] In case of an absolute error, the capital letter E is used in the following.

measurement, the data sheet of the crystal or oscillator can be used. Usually, this is only possible with self-built devices. Commercial devices often give very little information about the timing characteristics. In this case, a measurement has to be performed, e.g. comparing with an atomic clock via the Internet (network time protocol).

A different strategy is used for the estimation of uncertainties of voltage and current. The calibration uncertainty is specified in the data sheet of the measuring instrument or, if additional calibration devices are used, e.g. a precision benchtop multimeter, in that data sheet. The noise characteristic can be calculated directly as the standard deviation of the measured values. Time-drift and temperature induced uncertainties can be extracted from the data sheets of the relevant electronic components for self-built equipment. However, it can also be measured by changing the temperature of the instrument and evaluating the drift over time for successive calibrations. For commercial devices, this is usually the only way to obtain this data.

Finally, there are the following ways to reduce uncertainty. Calibration uncertainty can be improved by using better (more accurate) calibration equipment. Temperature-related effects can be reduced by placing the measuring equipment in a (tightly) controlled temperature chamber. Averaging over multiple samples can reduce noise, albeit by reducing the sample rate. Finally, time-drift is a basic property of the measuring device and cannot really be improved — without modification of the hardware itself.

3.2. Specification of the measurement equipment

In order to be able to give realistic example values, a self-built high-precision test setup consisting of a linear-controlled temperature chamber containing the battery cycler and battery is used as a reference.[2]

To suppress external disturbances, especially from the grid, the measuring time (integration time) for current and voltage measurements is selected to be exactly one main period ($T_{\text{grid}} = 20\,\text{ms}$, $f_{\text{grid}} = 50\,\text{Hz}$). Additionally, to achieve the desired high precision, a continuous offset and gain calibration is performed for both, the voltage and current measurement. This gives an overall sampling rate of $f_{\text{sample}} = 20\,\text{Hz}$. Temperatures are measured with the same data rate.

A digital controller is used to keep the temperature inside the chamber constant at $\vartheta_{\text{air}} = 40\,°\text{C}$. The temperature fluctuations (noise) have been measured as $u_{\vartheta\text{chamber}} = 60\,\text{mK}$. Part of the measurement electronics (shunt and voltage-reference) have an additional heating circuit, locally reducing the temperature variability to $u_{\vartheta\text{shuntAndRef}} = 6\,\text{mK}$. Due to the digital temperature control, only a very small temperature drift over time could be observed ($s_{\text{td}} < 0.05\,\text{mK/h}$). Considering the duration of a single charge/discharge of $T_{\text{cycle}} \approx 8\,\text{h}$, this results in a time-drift related uncertainty of

$$u_{\text{td,one cycle}} = s_{\text{td}} \cdot T_{\text{cycle}} \approx 0.05\,\frac{\text{mK}}{\text{h}} \cdot 8\,\text{h} = 0.4\,\text{mK} \tag{19}$$

Compared with $u_{\vartheta\text{chamber}}$ and $u_{\vartheta\text{shuntAndRef}}$, this influence can be neglected.

The corresponding uncertainties for the measurement of voltage, current, and time are shown in Table 1. Initial calibration for voltage and current measurement was performed using a $6\frac{1}{2}$ digit benchtop multimeter.

To reduce the influence of the voltage noise, the measuring equipment does not use the voltage values directly, but rather a linear approximation over 10 s measuring time ($N_{\text{interpolation}} = 200$ values). This regression line is then used to predict the intersection with V_{high} and V_{low}, but with an increased temporal resolution of $T_{\text{crossing}} = 1\,\text{ms}$, which also reduces the temporal uncertainty compared to the 20 ms standard sampling time.

[2] This setup has also been used to generate the plots in Section 2.

Table 1
Uncertainties and cross-sensitivities of the used measurement equipment.

	Calibration uncertainty $u_{\text{c,x}}$	Time-drift sensitivity $s_{\text{td,x}}$	Temperature sensitivity $s_{\vartheta,\text{x}}$	Noise uncertainty $u_{\text{n,x}}$
Voltage V	25 ppm	0.01 ppm/h	3 ppm/K	11 µV
Current I	700 ppm	0.02 ppm/h	23 ppm/K	38 µA
Time t	12 ppm	3 ppm/year	1 ppm/K	11 ns[a]

[a]For a sample time of 1 ms.

3.3. Battery

As shown in Figs. 1 and 5, the current I through the battery is imprinted by the test equipment and the corresponding voltage response V of the battery is measured. Using the simplified battery model shown in Fig. 3b, the voltage response can be divided into its contribution from the open circuit voltage OCV and the voltage drop across the internal resistance R:

$$V = OCV(SOC, t, N, \vartheta, p) + I \cdot R(SOC, t, N, \vartheta, p) \tag{20}$$

Voltage and resistance have various influencing factors, namely state-of-charge SOC, time t (age of the battery), number of cycles N, temperature ϑ and pressure p. Therefore, the stability (variability) of temperature and pressure during the measurement determines the uncertainty $u_{\text{V},\vartheta\text{p}}$:

$$u_{\text{V},\vartheta\text{p}} = \sqrt{\left(\frac{\partial V}{\partial \vartheta} \cdot u_{\vartheta}\right)^2 + \left(\frac{\partial V}{\partial p} \cdot u_{\text{p}}\right)^2} \tag{21}$$

Since the cell used for the example is of the cylindrical type, the pressure cannot be influenced by clamping the cell as is the case, for example, with a pouch-bag cell. For the calculation example, the second term in (21) can therefore be omitted leading to[3]:

$$u_{\text{V},\vartheta} = \left|\frac{\partial OCV}{\partial \vartheta} + I \cdot \frac{\partial R}{\partial \vartheta}\right| \cdot u_{\vartheta} = |TCV + I \cdot R \cdot TCR| \cdot u_{\vartheta} \tag{22}$$

Typical temperature dependence of the open circuit voltage – TCV (temperature coefficient of voltage) – is in the range of a few millivolt per Kelvin, and the internal resistance increases about a percent per Kelvin [24]. For the cell under consideration, it has been measured as $TCV_{\text{full}} = +0.2\,\text{mV/K}$ for the fully charged battery and $TCV_{\text{empty}} = -0.38\,\text{mV/K}$ for the empty one, respectively. For the internal resistance (at 50 % state of charge) a temperature coefficient of resistance $TCR = -0.05\,\%/\text{K}$ has been measured. With the data from Sections 2.3 and 3.2 this gives

$$u_{\text{Vhigh},\vartheta} = |0.2\,\text{mV/K} + 0.875\,\text{A} \cdot 63.7\,\text{m}\Omega \cdot (-0.05\,\%/\text{K})| \cdot 60\,\text{mK} = 10\,\mu\text{V} \tag{23}$$

for the full cell and

$$u_{\text{Vlow},\vartheta} = |-0.38\,\text{mV/K} + (-0.875\,\text{A}) \cdot 63.7\,\text{m}\Omega \cdot (-0.05\,\%/\text{K})| \cdot 60\,\text{mK} = 21\,\mu\text{V} \tag{24}$$

for the empty one, respectively. Note that the temperature dependence of the resistor was measured at 50 % SOC, as this is the only possibility, while it is used to predict the behavior at 0 and 100 % SOC. Therefore, some inaccuracies may occur.

[3] Of course, in the case of a pouch-bag or rectangular cell format where the external pressure/clamping affects the internal cell pressure, an analysis similar to that shown for temperature dependence must be performed.

4. Uncertainty analysis of the data analysis methods

In the following is the main part of this work – a detailed uncertainty analysis for each of the methods mentioned in Section 2. Each analysis is performed separately for the constant u_{const} and variable part u_{var} of the uncertainty.

4.1. Capacity

Eq. (1) can be evaluated as

$$Q_{discharge} = \int_{t_0}^{t_1} I \, dt = \bar{I} \cdot (t_1 - t_0) = \bar{I} \cdot T \tag{25}$$

with $\bar{I}$ the mean value of the discharge current and T the corresponding time duration of current flow. As can be seen from Fig. 1 the switching times t_0 and t_1 are defined by the intersection of the battery's voltage with the predefined voltage thresholds V_{low} and V_{high}. To simplify the further analysis, the time values t_0 and t_1 are shifted, so that t_0 is equal to zero, therefore, the variable for time t runs from 0 to T.

For the uncertainty analysis, the voltage and its influence on the switching time is examined first. Then we will add the uncertainties of current and time measurements to calculate the total uncertainty of the discharge capacity.

4.1.1. Variable part of uncertainty (capacity)

The measured voltage is subject to uncertainties due to both the accuracy of the measurement equipment (Section 3.2) and the effects of the battery (Section 3.3). For the fully charged cell, the variable part of the uncertainty for the voltage limit V_{high} is (similarly to Eq. (17), but most of the uncertainties in Table 1 are given relative to the measured value)

$$u_{var,Vhigh} = \sqrt{(s_{\vartheta,V} \cdot u_{\vartheta shuntAndRef} \cdot V_{high})^2 + \frac{u_{n,V}^2}{N_{interpolation}} + u_{Vhigh,\vartheta}^2}$$
$$= \sqrt{(0.08\,\mu V)^2 + (0.8\,\mu V)^2 + (10\,\mu V)^2} = 10\,\mu V \tag{26}$$

The voltage slope at end of charge has been measured as $m_{Vhigh} = 0.1\,mV/s$. This leads to a corresponding uncertainty in time

$$u_{var,t,Vhigh} = \frac{u_{var,Vhigh}}{|m_{Vhigh}|} = \frac{10\,\mu V}{0.1\,mV/s} = 100\,ms \tag{27}$$

Similarly, for the end of discharge, with discharge time $T \approx 221\,min$ this gives

$$u_{var,Vlow} = \{(s_{td,V} \cdot T \cdot V_{low})^2 + (s_{\vartheta,V} \cdot u_{\vartheta shuntAndRef} \cdot V_{low})^2 + \frac{u_{n,V}^2}{N_{interpolation}} + u_{Vlow,\vartheta}^2\}^{1/2} \tag{28}$$
$$= \sqrt{(0.09\,\mu V)^2 + (0.05\,\mu V)^2 + (0.8\,\mu V)^2 + (21\,\mu V)^2} = 21\,\mu V \tag{29}$$

The voltage slope at end of discharge is $m_{Vlow} = -2.3\,mV/s$, which gives an uncertainty in time for detecting the lower threshold V_{low} of $u_{var,t,Vlow} = 9\,ms$.

Additionally, the uncertainty of the time measurement itself has to be considered as well. Each single time-slot of length $T_{sample,time} = 1\,ms$ has associated uncertainty

$$u_{timeslot}(t) = \sqrt{(s_{td,t} \cdot t \cdot T_{sample,time})^2 + (s_{\vartheta,t} \cdot u_{\vartheta chamber} \cdot T_{sample,time})^2 + u_{n,t}^2} \tag{30}$$

The intersection of the voltages occurs inside a single time-slot at the beginning and end of the discharge period, respectively, resulting in additional uncertainty of

$$u_{intersection} = \sqrt{\frac{T_{sample,time}^2}{12} + \frac{T_{sample,time}^2}{12}} = \frac{T_{sample,time}}{\sqrt{6}} \tag{31}$$

The total time duration $T = t_1 - t_0$ consists of the sum of $M = T/T_{sample,time}$ samples leading to an overall uncertainty of (see also Appendix A for the derivation of Eq. (32))

$$u_{var,T} = \{s_{td,t}^2 \cdot T_{sample,time} \cdot \frac{T^3}{3} + M \cdot s_{\vartheta,t}^2 \cdot u_{\vartheta chamber}^2 \cdot T_{sample,time}^2 + M \cdot u_{n,t}^2 + \frac{T_{sample,time}^2}{6}\}^{1/2} \tag{32}$$
$$= \{(0.003\,\mu s)^2 + (0.22\,\mu s)^2 + (40\,\mu s)^2 + (408\,\mu s)^2\}^{1/2} = 0.41\,ms \tag{33}$$

Overall, this gives a variable uncertainty in time $u_{var,T,total}$ of

$$u_{var,T,total} = \sqrt{u_{var,t,Vhigh}^2 + u_{var,t,Vlow}^2 + u_{var,T}^2} = \tag{34}$$
$$= \sqrt{(100\,ms)^2 + (9\,ms)^2 + (0.41\,ms)^2} = 0.1\,s \tag{35}$$

The current I has associated uncertainties of

$$u_{var,I}(t) = \sqrt{(s_{td,I} \cdot t \cdot I)^2 + (s_{\vartheta,I} \cdot u_{\vartheta shuntAndRef} \cdot I)^2 + u_{n,I}^2} \tag{36}$$

which for the average current $\bar{I}$ gives (see also Appendix B for the derivation of Eq. (37))

$$u_{var,\bar{I}} = \sqrt{\frac{(s_{td,I} \cdot T \cdot I)^2}{3 \cdot M} + \frac{(s_{\vartheta,I} \cdot u_{\vartheta shuntAndRef} \cdot I)^2}{M} + \frac{u_{n,I}^2}{M}}$$
$$= \sqrt{(0.07\,nA)^2 + (0.2\,nA)^2 + (74\,nA)^2} = 74\,nA \tag{37}$$

Overall, this leads to an uncertainty for the discharge capacity u_Q

$$u_Q = \sqrt{\left(\frac{\partial Q}{\partial I} \cdot u_I\right)^2 + \left(\frac{\partial Q}{\partial T} \cdot u_T\right)^2} \tag{38}$$

$$u_{var,Q} = \sqrt{(T \cdot u_{var,\bar{I}})^2 + (I \cdot u_{var,T,total})^2}$$
$$= \sqrt{(0.98\,mAs)^2 + (88\,mAs)^2} = 88\,mAs = 0.024\,mAh \tag{39}$$

$$\frac{u_{var,Q}}{Q} = \frac{0.024\,mAh}{3100\,mAh} = 7.8\,ppm \tag{40}$$

To check the correctness of this value, let us compare it with the actual measurement noise. Starting from the data shown in Fig. 2a, the overall curve is approximated by a polynomial of order 8 which is then subtracted. The remaining signal (Fig. 6a) – the noise – has a standard deviation of 0.024 mAh, which is identical to the predicted value. It can therefore be assumed, that the performed calculation represents the real behavior very well and can be used to identify the main contributors. For this, the uncertainty analysis is traversed in reverse order:

- $u_{var,Q}$ is dominated by $u_{var,T,total}$, which in turn is dominated by $u_{var,t,Vhigh}$ and $u_{var,t,Vlow}$.
- $u_{var,t,Vhigh}$ and $u_{var,t,Vlow}$ are dominated by $u_{Vhigh,\vartheta}$ and $u_{Vlow,\vartheta}$. However, this is only the case because the battery voltage is not used directly to predict the voltage transitions, but a linear approximation (regression line) is used. If this were not the case, then in Eqs. (26) and (28) the term $u_{n,V}^2/N_{interpolation}$ would become $u_{n,V}^2$ and the influence would be similar to the influence of $u_{Vhigh,\vartheta}$ and $u_{Vlow,\vartheta}$. Commercial measurement devices typically do not have this feature, so a limit would be reached in this case.
- $u_{Vhigh,\vartheta}$ and $u_{Vlow,\vartheta}$ depend on parameters given by the battery itself and the quality of temperature control. Since the battery parameters cannot be changed, the only way to further improve the overall result would be to enhance the temperature control itself.

4.1.2. Constant part of uncertainty (capacity)

Using a time T_c of, for example, one month between calibration and measurement, Eq. (16) gives

$$u_{c,total,V} = \sqrt{(25\,ppm)^2 + (7.3\,ppm)^2} = 26\,ppm \tag{41}$$

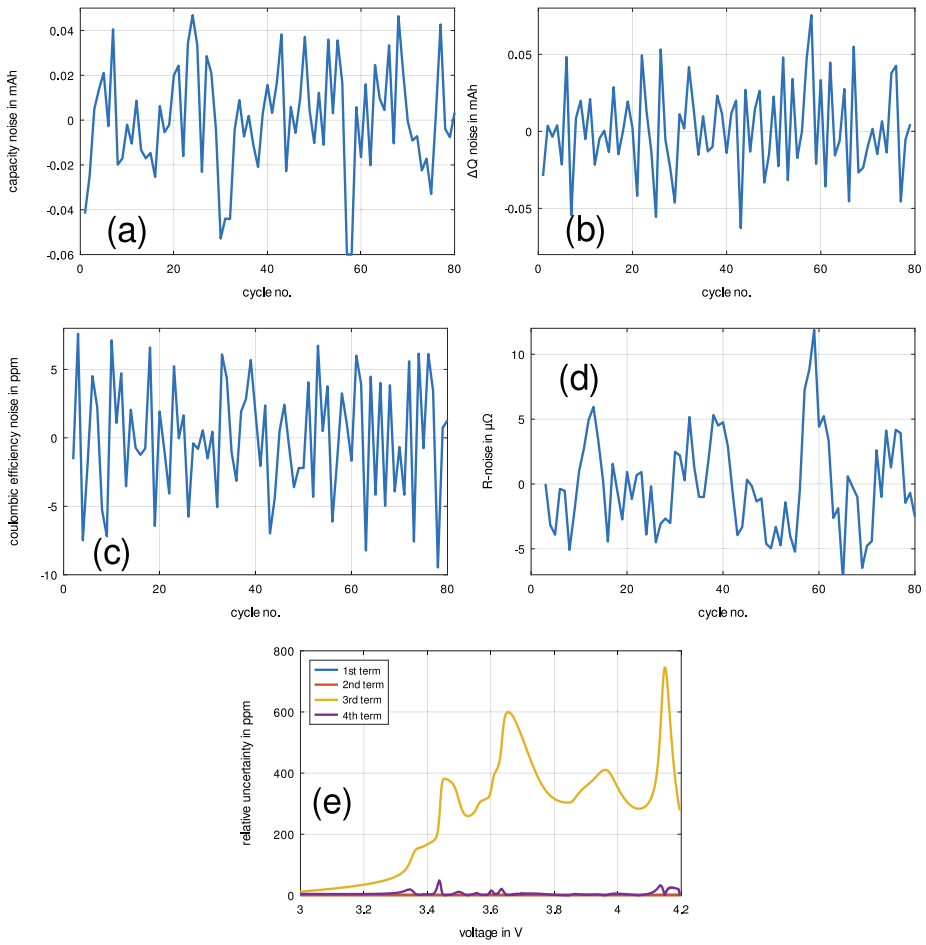

Fig. 6. (a) Noise of the battery discharge capacity measurement of the LG MJ1 cell at 40 °C. (b) Noise of the change-of-capacity ΔQ measurement. (c) Noise of the Coulombic efficiency measurement. (d) Noise of internal resistance measurement. (e) Contributions of the individual terms in Eq. (88).

$$u_{\mathrm{c,total,I}} = \sqrt{(700\,\mathrm{ppm})^2 + (15\,\mathrm{ppm})^2} = 700\,\mathrm{ppm} \tag{42}$$

$$u_{\mathrm{c,total,t}} = \sqrt{(12\,\mathrm{ppm})^2 + (0.25\,\mathrm{ppm})^2} = 12\,\mathrm{ppm} \tag{43}$$

Overall, the drift is more or less negligible in one month. Increasing the time after calibration to one year, there is still almost no influence on the current (because the calibration uncertainty is so large) and the time measurement (because the drift is so small). Only for the voltage measurement a significant increase would be observable. Commercially available high-precision instruments usually show similar results, with the instrument usually needing to be recalibrated once a year.

Then, with the absolute errors E_{x} in time

$$E_{\mathrm{t,Vhigh}} = \frac{V_{\mathrm{high}} \cdot (1 + e_{\mathrm{V}})}{m_{\mathrm{Vhigh}}} \tag{44}$$

$$E_{\mathrm{t,Vlow}} = \frac{V_{\mathrm{low}} \cdot (1 + e_{\mathrm{V}})}{m_{\mathrm{Vlow}}} \tag{45}$$

$$E_{\mathrm{T}} = t_2 \cdot (1 + e_T) - t_1 \cdot (1 + e_T) = T \cdot (1 + e_T) \tag{46}$$

$$E_{\mathrm{T,total}} = E_{\mathrm{t,Vhigh}} + E_{\mathrm{t,Vlow}} + E_{\mathrm{T}} \tag{47}$$

one can substitute the relative errors e_{x} with the corresponding uncertainties and calculate the total uncertainty in time

$$u_{\mathrm{const,T,total}} = \sqrt{\left[\left(\frac{V_{\mathrm{high}}}{m_{\mathrm{Vhigh}}} + \frac{V_{\mathrm{low}}}{m_{\mathrm{Vlow}}}\right) \cdot u_{\mathrm{c,total,V}}\right]^2 + T^2 \cdot u^2_{\mathrm{c,total,t}}}$$

$$= \sqrt{(1.1\,\mathrm{s})^2 + (0.16\,\mathrm{s})^2} = 1.1\,\mathrm{s} \tag{48}$$

Finally, the constant part of the uncertainty for the discharge capacity is

$$u_{\mathrm{const,Q}} = \sqrt{(T \cdot u_{\mathrm{c,total,I}} \cdot I)^2 + (I \cdot u_{\mathrm{const,T,total}})^2}$$

$$= \sqrt{(8.1\,\mathrm{As})^2 + (0.96\,\mathrm{As})^2} = 8.2\,\mathrm{As} \tag{49}$$

and overall

$$u_{\mathrm{total,Q}} = \sqrt{u^2_{\mathrm{var,Q}} + u^2_{\mathrm{const,Q}}} = 8.2\,\mathrm{As} \tag{50}$$

For example, using a coverage factor of $k = 2$ (confidence level of approximately 95 %), the final result for cycle no. 2 ($T = 13247.342\,\mathrm{s}$) is therefore

$$Q_{\mathrm{discharge,2}} = 11591 \pm 16\,\mathrm{As} = 3220 \pm 4.6\,\mathrm{mAh} \tag{51}$$

Comparing $u_{\mathrm{var,Q}}$ (39) and $u_{\mathrm{const,Q}}$ (49), the calibration uncertainty of the current measurement dominates the total uncertainty. This typically also applies to measuring devices other than the one used in the example, since current measurement, compared to voltage and time measurement, usually has the greatest uncertainty.

4.2. Capacity change over time

To study the change in discharge capacity over time, the relative capacity decrease is typically used

$$\Delta Q_{\mathrm{relative,m,n}} = \frac{Q_{\mathrm{discharge,m}} - Q_{\mathrm{discharge,n}}}{Q_{\mathrm{discharge,n}}} = \frac{\bar{I}_{\mathrm{m}} \cdot T_{\mathrm{m}}}{\bar{I}_{\mathrm{n}} \cdot T_{\mathrm{n}}} - 1 \tag{52}$$

The further apart the cycles m (target) and n (reference) are from each other, the 'smoother' the resulting curve becomes, but it also takes longer (more cycles must be measured) until the first result is available. For the calculation example we will use $m = n+1$, the direct successor.

4.2.1. Constant part of uncertainty (capacity change over time)

Adding the error-terms to Eq. (52) leads to

$$\begin{aligned}\Delta Q_{\text{const error}} &= \frac{\bar{I}_\text{m}\cdot(1+e_\text{I})\cdot T_\text{m}\cdot(1+e_\text{t})}{\bar{I}_\text{n}\cdot(1+e_\text{I})\cdot T_\text{n}\cdot(1+e_\text{t})} - 1 \\ &= \frac{\bar{I}_\text{m}\cdot T_\text{m}}{\bar{I}_\text{n}\cdot T_\text{n}} - 1 = \Delta Q_{\text{relative,m,n}}\end{aligned} \tag{53}$$

Due to the division, the error-terms cancel each other out. The result is thus independent of the constant part of the uncertainty, i.e. calibration uncertainty, and only the variable part remains.

4.2.2. Variable part of uncertainty (capacity change over time)

The difference between m and n, and thus the time between the two capacity measurements, affects the parameters relevant to time drift. Therefore, the uncertainty values for the reference cycle n can be taken directly from Section 4.1, the values for the target cycle m must be adjusted accordingly. For the variable part of the uncertainty, with time $T_{\text{n,m}} = 2\cdot 221\,\text{min}$ (one charge plus discharge time) between the two measurements, this gives (see also Eqs. (34), (36) and (39))

$$u_{\text{var,T,total,m}} = \sqrt{(100\,\text{ms})^2 + (9\,\text{ms})^2 + (0.41\,\text{ms})^2} = 0.1\,\text{s} \tag{54}$$

$$u_{\text{var,}\bar{\text{I}}\text{,m}} = \sqrt{(64\,\text{nA})^2 + (0.2\,\text{nA})^2 + (74\,\text{nA})^2} = 98\,\text{nA} \tag{55}$$

$$\begin{aligned}u_{\text{var,Q,m,n}} = \Bigg(&\left(\frac{\partial\Delta Q}{\partial I_\text{m}}\cdot u_{\text{var,}\bar{\text{I}}\text{,m}}\right)^2 + \left(\frac{\partial\Delta Q}{\partial I_\text{n}}\cdot u_{\text{var,}\bar{\text{I}}\text{,n}}\right)^2 + \left(\frac{\partial\Delta Q}{\partial T_\text{m}}\cdot u_{\text{var,T,total,m}}\right)^2 \\ &+\left(\frac{\partial\Delta Q}{\partial T_n}\cdot u_{\text{var,T,total,n}}\right)^2\Bigg)^{1/2}\end{aligned} \tag{56}$$

Assuming $(\bar{I}_\text{m}\cdot T_\text{m})/(\bar{I}_\text{n}\cdot T_\text{n}) \approx 1$ this equation can be solved as

$$\begin{aligned}u_{\text{var,Q,m,n}} &= \Bigg\{\left(\frac{u_{\text{var,}\bar{\text{I}}\text{,m}}}{\bar{I}_\text{m}}\right)^2 + \left(\frac{u_{\text{var,}\bar{\text{I}}\text{,n}}}{\bar{I}_\text{n}}\right)^2 + \\ &\quad \left(\frac{u_{\text{var,T,total,m}}}{T_\text{m}}\right)^2 + \left(\frac{u_{\text{var,T,total,n}}}{T_\text{n}}\right)^2\Bigg\}^{1/2}\end{aligned} \tag{57}$$

$$= \sqrt{(0.1\,\text{ppm})^2 + (0.09\,\text{ppm})^2 + (7.5\,\text{ppm})^2 + (7.5\,\text{ppm})^2} = 11\,\text{ppm} \tag{58}$$

The main contribution stems from the last two terms in Eq. (58), which are more or less the same — no real influence of time-drift can be seen. Thus, the final result can also be approximated as

$$u_{\text{var,Q,m,n}} \approx \sqrt{2}\cdot\frac{u_{\text{var,T,total,n}}}{T_\text{n}} \tag{59}$$

As before, extracting the noise from the data in Fig. 2b leads to the data shown in Fig. 6b. This noise has a standard deviation of 29 µAh. Referred to the actual capacity of about 3100 mAh this results in 9.4 ppm relative standard deviation. As expected, this fits very well with the calculated value of 11 ppm. All conclusions shown at end of Section 4.1.1 are of course also valid here.

4.3. Coulombic efficiency

Handling of the Coulombic efficiency is similar to the 'capacity change over time' in the previous section, since both are ratios.

4.3.1. Constant part of uncertainty (Coulombic efficiency)

Expanding Q and adding the error-terms to Eq. (5) leads to

$$\begin{aligned}CE_{\text{const error}} &= \frac{\bar{I}_\text{discharge}\cdot(1+e_\text{I,discharge})\cdot T_\text{discharge}\cdot(1+e_\text{t})}{\bar{I}_\text{charge}\cdot(1+e_\text{I,charge})\cdot T_\text{charge}\cdot(1+e_\text{t})} \\ &= CE\cdot\frac{(1+e_\text{I,discharge})}{(1+e_\text{I,charge})}\end{aligned} \tag{60}$$

Since the current flow changes its direction, the error during charging $e_{\text{I,charge}}$ and discharging $e_{\text{I,discharge}}$ typically differs slightly, leaving a small deviation between the ideal Coulombic efficiency value CE and actual achievable $CE_{\text{const error}}$, which results in a small gain error in the final value. For specially designed hardware, as is the case for the equipment described in Section 3.2, this deviation is only a few ppm and can therefore be neglected, so $CE_{\text{const error}} \approx CE$ and only the variable part of the uncertainty is important.

4.3.2. Variable part of uncertainty (Coulombic efficiency)

The variable part of the uncertainty is calculated more or less the same as in Section 4.2.2 for Eq. (52). Instead of the ratio of two discharges, CE is calculated as the ratio of a discharge vs. a charge. The final '−1' is missing in the equation, but this has no influence on the uncertainty calculation. The main difference for the calculation lies in the fact, that the end of charge is identical with the begin of discharge. A shift of this point has the same effect on Q_{charge} and $Q_{\text{discharge}}$ and is therefore canceled out by the division — eliminating the influence of Eq. (27) ($u_{\text{var,t,Vhigh}}$), which, by the way, had the greatest influence on uncertainty. This significantly reduces $u_{\text{var,T,total}}$ from 100 ms to 9 ms and with the approximation of Eq. (59) this leads to an overall variable part for the uncertainty of

$$u_{\text{var,CE}} \approx \sqrt{2}\cdot\frac{9\,\text{ms}}{221\,\text{min}\cdot 60\,\text{s/min}} = 1\,\text{ppm} \tag{61}$$

As before, extracting and analyzing the noise from the data shown in Fig. 2c gives a standard deviation of 4.2 ppm (Fig. 6c). The measured and calculated values differ more than the results in Sections 4.1.1 and 4.2.2. However, they are similar enough to still be able to draw conclusions about the causes of the uncertainty. This time, the main contribution stems from Eq. (24) $u_{\text{Vlow,}\vartheta}$, the uncertainty of the battery voltage at V_{low} due to temperature cross-sensitivity. Therefore, also here the temperature control of the battery plays an important role.

4.4. Internal resistance

To calculate the uncertainty of the internal resistance R from Eq. (7), the uncertainties of current, charge and voltage are needed first. Main difference to the previous calculations is that the averaging is only carried out over a small time range, i.e. $T_{\text{avg}} < T$ (in the example of Section 2.3 $T_{\text{avg}} = T/10$). Again the calculation is split into a constant and variable part:

4.4.1. Constant part of uncertainty (internal resistance)

Adding the error-terms to Eq. (7) leads to[4]

$$R_{\text{const error}} = \frac{\overline{V}_{\text{charge,r}}\cdot(1+e_\text{V}) - \overline{V}_{\text{discharge,r}}\cdot(1+e_\text{V})}{2\cdot\bar{I}_\text{r}\cdot(1+e_\text{I})} = R\cdot\frac{(1+e_\text{V})}{(1+e_\text{I})} \tag{62}$$

and with the values from Section 4.1.2 this gives

$$u_{\text{const,R}} = \sqrt{u_{\text{c,total,V}}^2 + u_{\text{c,total,I}}^2} = 700\,\text{ppm} \tag{63}$$

which again shows, that the uncertainty of the current measurement dominates the constant part of the uncertainty.

4.4.2. Variable part of uncertainty (internal resistance)

Eq. (7) depends on the average voltage and current in a given charge range r. This charging range is defined in relation to the actual capacity of the cell during the charging and discharging. Therefore, the

[4] Due to the averaging over a considerable charge range, the influence of the uncertainty of the state of charge Q on the voltage is neglected.

uncertainty of the charge range r depends on both, the limits of the total capacity and the accuracy of cutting out the specific charge range itself

$$u_{\mathrm{cutout}} = T_{\mathrm{sample}}/\sqrt{12} \tag{64}$$

Similar to the uncertainty calculation of the Coulombic efficiency, when measuring the internal resistance, the charge and the discharge share the same upper voltage point V_{high}, which can therefore be eliminated, resulting in an uncertainty in time of (see also Eq. (34))

$$u_{\mathrm{var,r,t}} = \sqrt{u^2_{\mathrm{var,t,Vlow}} + u^2_{\mathrm{var,T}} + 2\cdot u^2_{\mathrm{cutout}}} \tag{65}$$

$$= \sqrt{(9\,\mathrm{ms})^2 + (0.41\,\mathrm{ms})^2 + 2\cdot(14\,\mathrm{ms})^2} = 22\,\mathrm{ms} \tag{66}$$

multiplying by the average current and DVA, this gives

$$u_{\mathrm{var,r,V}} = u_{\mathrm{var,r,t}}\cdot \bar{I}\cdot \overline{DVA}_{\mathrm{r}} = 22\,\mathrm{ms}\cdot 0.875\,\mathrm{A}\cdot 76\,\mu\mathrm{V/As} = 1.5\,\mu\mathrm{V} \tag{67}$$

Overall, this gives a voltage uncertainty of

$$u_{\mathrm{var},\bar{V}} = \{(s_{\mathrm{td,V}}\cdot T\cdot \bar{V}_{\mathrm{r}})^2 + (s_{\vartheta,\mathrm{V}}\cdot u_{\vartheta\mathrm{shuntAndRef}}\cdot \bar{V}_{\mathrm{r}})^2 + \frac{T_{\mathrm{sample}}}{T_{\mathrm{avg}}}\cdot u^2_{\mathrm{n,V}} + 2\cdot u^2_{\mathrm{var,r,V}}\}^2 \tag{68}$$

$$= \sqrt{(0.14\,\mu\mathrm{V})^2 + (0.07\,\mu\mathrm{V})^2 + (0.07\,\mu\mathrm{V})^2 + (2.1\,\mu\mathrm{V})^2} = 2.1\,\mu\mathrm{V} \tag{69}$$

For the uncertainty of the average current, Eq. (37) can be used, but with a shorter duration for the average time calculation ($T_{\mathrm{avg}} = T/10$), which gives $u_{\mathrm{var},\bar{I}} = 0.23\,\mu\mathrm{A}$.

Overall, for the variable part of the resistance uncertainty one gets

$$\frac{u_{\mathrm{var,R}}}{R} = \sqrt{2\cdot\left(\frac{u_{\mathrm{var},\bar{V}}}{\overline{V}_{\mathrm{charge,r}} - \overline{V}_{\mathrm{discharge,r}}}\right)^2 + \left(\frac{u_{\mathrm{var},\bar{I}}}{\bar{I}_{\mathrm{r}}}\right)^2}$$

$$= \sqrt{(27\,\mathrm{ppm})^2 + (0.26\,\mathrm{ppm})^2} = 27\,\mathrm{ppm} \tag{70}$$

$$u_{\mathrm{var,R}} = 63.7\,\mathrm{m}\Omega\cdot 27\,\mathrm{ppm} = 1.7\,\mu\Omega \tag{71}$$

The main contributions to this noise stem from $u_{\mathrm{Vlow},\vartheta}$, Eq. (24) and u_{cutout}, Eq. (64). As with the uncertainty analysis of the Coulombic efficiency in Section 4.3.2, moist probably due to the involvement of $u_{\mathrm{Vlow},\vartheta}$, a discrepancy between calculated (1.7 μΩ) and observed noise (3.7 μΩ, Fig. 6d) can be seen.

4.5. Differential capacity analysis

When calculating the differential capacitance, see Eq. (8)

$$DCA_x = \left.\frac{\mathrm{d}Q}{\mathrm{d}V}\right|_x \approx \frac{\Delta Q_x}{\Delta V_x} = \frac{\bar{I}\cdot(t_{x+1}-t_x)}{V_{x+1}-V_x} = \frac{\bar{I}\cdot\Delta t}{V_{x+1}-V_x} \tag{72}$$

the change of charge Q and voltage V over time is used, thus highlighting the noise. To prevent this, it is necessary to low-pass filter the signals first. Since the higher frequency components are removed, the number of points can be reduced by downsampling, making it also easier to manage the data.

For Fig. 4 a moving average filter of length $N = 800$, followed by downsampling by the same ratio N has been used, resulting in a reduced sample rate of

$$\Delta t = T_{\mathrm{sample}}\cdot N = 50\,\mathrm{ms}\cdot 800 = 40\,\mathrm{s} \tag{73}$$

The filter length was chosen so that the average voltage change $\overline{\Delta V_{\mathrm{x}}}$ still has a 'good' resolution (≈ 2.5 mV).

In principle, one would also have to consider the influence of the x-axis (voltage) for the uncertainty analysis. But since this would only lead to a negligible shift of the DCA values on the x-axis, this influence is neglected in the following.

4.5.1. Constant part of uncertainty (DCA)

Starting by inserting the error-terms into Eq. (72) first

$$DCA_{\mathrm{const\ error}} = \frac{\bar{I}\cdot(1+e_I)\cdot[t_{x+1}\cdot(1+e_t) - t_x\cdot(1+e_t)]}{V_{x+1}\cdot(1+e_V) - V_x\cdot(1+e_V)} = \frac{\bar{I}\cdot(t_{x+1}-t_x)}{V_{x+1}-V_x}\cdot\frac{(1+e_I)\cdot(1+e_t)}{(1+e_V)} \tag{74}$$

the constant part of the uncertainty becomes

$$u_{\mathrm{const,DCA}} = \sqrt{u^2_{\mathrm{c,total,I}} + u^2_{\mathrm{c,total,t}} + u^2_{\mathrm{c,total,V}}} = 701\,\mathrm{ppm} \tag{75}$$

4.5.2. Variable part of uncertainty (DCA)

The average current $\bar{I}$ in Eq. (72) can be handled similarly to Section 4.1, but with shorter duration Δt. So, substituting T with Δt in Eq. (37) gives

$$u_{\mathrm{var},\bar{I}} = \sqrt{(0.1\,\mathrm{nA})^2 + (0.004\,\mu\mathrm{A})^2 + (1.3\,\mu\mathrm{A})^2} = 1.3\,\mu\mathrm{A} \tag{76}$$

Similarly, for the uncertainty of the duration Δt Eq. (32) can be used, but omitting the last term related to $u_{\mathrm{intersection}}$

$$u_{\mathrm{var},\Delta t} = \sqrt{(0.4\,\mathrm{ps})^2 + (0.012\,\mu\mathrm{s})^2 + (2.2\,\mu\mathrm{s})^2} = 2.2\,\mu\mathrm{s} \tag{77}$$

Finally, repeating the steps shown in Section 4.4.2 for $u_{\mathrm{var},\bar{V}}$, but with $T_{\mathrm{avg}} = \Delta t$ and an average cell voltage $\bar{V} = 3.7\,\mathrm{V}$

$$u_{\mathrm{var},\bar{V}} = \sqrt{2}\cdot\{(s_{\vartheta,\mathrm{V}}\cdot u_{\vartheta\mathrm{shuntAndRef}}\cdot\bar{V})^2 + \frac{T_{\mathrm{sample}}}{T_{\mathrm{avg}}}\cdot u^2_{\mathrm{n,V}}\}^{1/2} \tag{78}$$

$$= \sqrt{2}\cdot\sqrt{(0.07\,\mu\mathrm{V})^2 + (0.39\,\mu\mathrm{V})^2} = 0.56\,\mu\mathrm{V} \tag{79}$$

Overall this gives a variable uncertainty of

$$\frac{u_{DCA,\mathrm{x}}}{DCA_{\mathrm{x}}} = \sqrt{\left(\frac{u_{\mathrm{var},\bar{I}}}{\bar{I}}\right)^2 + \left(\frac{u_{\mathrm{var},\Delta t}}{\Delta t}\right)^2 + \left(\frac{u_{\mathrm{var},\bar{V}}}{\Delta V_{\mathrm{x}}}\right)^2} \tag{80}$$

This uncertainty depends on ΔV_{x}, but to make a first estimate, the smallest and largest ΔV_x are used (1.3 mV and 3.8 mV)

$$\frac{u_{DCA,\mathrm{x}}}{DCA_{\mathrm{x}}} > \sqrt{(1.5\,\mathrm{ppm})^2 + (0.06\,\mathrm{ppm})^2 + (147\,\mathrm{ppm})^2} = 147\,\mathrm{ppm} \tag{81}$$

$$\frac{u_{DCA,\mathrm{x}}}{DCA_{\mathrm{x}}} < \sqrt{(1.5\,\mathrm{ppm})^2 + (0.06\,\mathrm{ppm})^2 + (431\,\mathrm{ppm})^2} = 431\,\mathrm{ppm} \tag{82}$$

showing that, even for the largest ΔV_{x} the last term is clearly dominant, which subsequently leads to the prevailing influencing factor from Eq. (78), the voltage noise $u_{\mathrm{n,V}}$.

4.6. Delta differential capacity analysis

ΔDCA, as shown in Eq. (10), is essentially the difference of two DCA-measurements. Thus, the analysis is more or less the same as the procedure shown in Section 4.5, but because of the time difference between the two DCA-measurements, drift effects must be accounted for appropriately. In addition, the uncertainty of the x-axis (voltage) must now also be taken into account, since even small drifts can lead to significant differences between the two DCA values.

4.6.1. Constant part of uncertainty (Delta-DCA)

Since the result is computed as difference of two DCA-values, the corresponding uncertainty is simply

$$u_{\mathrm{const},\Delta\mathrm{DCA}} = \sqrt{2}\cdot u_{\mathrm{const,DCA}} = 0.1\% \tag{83}$$

4.6.2. Variable part of uncertainty (Delta-DCA)

The variable uncertainty for DCA_{ref} can be taken directly from Section 4.5.2, but for $DCA_{\mathrm{ref+N}}$ the drift effects during the N cycles must be taken into account. Using $N = 5$, as in Section 2.4 gives

$$u_{\mathrm{var},\bar{I},\mathrm{N}} = \sqrt{(0.19\,\mu\mathrm{A})^2 + (0.004\,\mu\mathrm{A})^2 + (1.3\,\mu\mathrm{A})^2} = 1.3\,\mu\mathrm{A} \tag{84}$$

$$u_{\mathrm{var},\Delta t,\mathrm{N}} = \sqrt{(0.03\,\mu\mathrm{s})^2 + (0.012\,\mu\mathrm{s})^2 + (2.2\,\mu\mathrm{s})^2} = 2.2\,\mu\mathrm{s} \tag{85}$$

$$u_{\mathrm{var},\bar{\mathrm{V}},\mathrm{N}} = \sqrt{2}\cdot\sqrt{(0.39\,\mu\mathrm{V})^2 + (0.07\,\mu\mathrm{V})^2 + (0.39\,\mu\mathrm{V})^2} = 0.79\,\mu\mathrm{V} \tag{86}$$

Only for $u_{\mathrm{var},\bar{\mathrm{V}}}$ a slight increase can be observed.

In addition, the effects of uncertainty in voltage to the x-axis must be taken into account

$$u_{\mathrm{var,DCA,V}} = \frac{\mathrm{d}DCA}{\mathrm{d}V}\cdot\sqrt{u^2_{\mathrm{var},\bar{\mathrm{V}}} + u^2_{\mathrm{var},\bar{\mathrm{V}},\mathrm{N}}} \tag{87}$$

Therefore, the variable uncertainty is

$$u_{\Delta DCA,\mathrm{x}} = \Delta DCA_{\mathrm{x}}\cdot\left(\frac{u^2_{\mathrm{var},\bar{\mathrm{I}}} + u^2_{\mathrm{var},\bar{\mathrm{I}},\mathrm{N}}}{\bar{I}^2} + \frac{u^2_{\mathrm{var},\Delta t} + u^2_{\mathrm{var},\Delta t,\mathrm{N}}}{\Delta t^2} + \frac{u^2_{\mathrm{var},\bar{\mathrm{V}}} + u^2_{\mathrm{var},\bar{\mathrm{V}},\mathrm{N}}}{\Delta V^2_{\mathrm{x}}} + \frac{u^2_{\mathrm{var,DCA,V}}}{DCA^2}\right)^{1/2} \tag{88}$$

Fig. 6e shows the individual contributions of the 4 terms in Eq. (88). The 3rd term – the uncertainty of the voltage – clearly dominates. Looking at Eq. (78), despite the high filtering of the input data, the voltage noise itself is still the dominant influencing factor. Then again, the total uncertainty is less than 0.08%, which is still an excellent result.

4.7. Differential voltage analysis and Delta-DVA

DVA is the reciprocal of *DCA*, Eq. (11). Therefore the (relative) uncertainties are the same as for DCA and Delta-DCA shown in Sections 4.5 and 4.6, respectively. There is a slight difference because the x-axis is not the cell voltage anymore, but the state of charge. But as shown above, the voltage uncertainty with respect to the x-axis plays only a minor role, and without showing it in detail here, the same is true in the case when the state of charge is used as the x-axis. This effect can therefore still be neglected.

5. Summary and conclusion

In this paper, a thorough analysis of the uncertainty for different state-of-the-art measurement methods and practical values of the uncertainties to be expected when performing these measurements with a modern high precision measuring instrument are given. These results, which are summarized in Table 2, also show the main influencing factors — and thus how the results could be even further improved.

For the analysis, we divided the overall uncertainty into two parts – a constant and a variable part. The constant part is essentially responsible for the absolute achievable accuracy and depends mainly on the accuracy of the calibration equipment used. This value must be taken into account when making absolute statements, e.g. what capacity (in mAh) does the cell have? In contrast, when analyzing the change in the cell over time, i.e., observing individual values over time or cycles, it is mainly the variable part of the uncertainty that is of interest.

In the example shown, a $6\frac{1}{2}$ digit benchtop multimeter is used for calibration. Since, as is typically the case for high-end instruments, the current measurement has a much higher uncertainty than the voltage measurement (more than an order of magnitude difference), for the constant part of uncertainty, current-measurement is the dominant contribution (the values of $u_{\mathrm{c,I}}$ in Table 2 are > 99%).

For the variable part of uncertainty, the situation is somewhat more varied. For the analysis methods of capacity, capacity change, and Coulombic efficiency, $u_{\mathrm{Vhigh},\vartheta}$ and $u_{\mathrm{Vlow},\vartheta}$ play the dominant role. From Eqs. (23) and (24), it is evident, that $u_{\mathrm{Vhigh},\vartheta}$ and $u_{\mathrm{Vlow},\vartheta}$ depend directly on the characteristics of the battery (temperature dependence of open-circuit voltage and internal resistance) and the temperature stability of the battery's temperature chamber. The used temperature chamber has a precision (noise, variability) of ±0.1 °C. So to further increase the precision of these measurements, an even more stable temperature chamber must be used. In the case of internal resistance, an additional factor (u_{cutout}) comes into play. Overall, however, the variable portion of the uncertainty for these four methods is only a few ppm to a few tens of ppm, which is certainly sufficient for most applications. Note that this good result is partially possible only due to the special filtering of the voltage signal, i.e. using a regression line to detect the voltage transition, as described at the end of Section 4.1.1, otherwise the contribution of $u_{\mathrm{n,V}}$ would be in a similar range as $u_{\mathrm{Vhigh},\vartheta}$ and $u_{\mathrm{Vlow},\vartheta}$. As far as the authors know, only the (self-built) device in this work has this feature, commercial devices do not. For the remaining four methods (DCA, DVA, ΔDCA, ΔDVA), the main contributions come from voltage noise $u_{\mathrm{n,V}}$ and drift over time $s_{\mathrm{td,V}}\cdot T$, although quite strong filtering is used (see Section 4.5). Even if the achievable values of uncertainty are much worse (hundreds of ppm), they are still less than '0.1%',[5] thus indicating very accurate measurements.

Overall, modern high-precision measuring equipment enables very precise and accurate measurements. However, to achieve good results the battery must be operated in a stabilized environment (temperature chamber).

CRediT authorship contribution statement

Bernhard Schweighofer: Conceptualization, Methodology, Software, Investigation, Writing – original draft, Writing – review & editing, Visualization. **Daniel Schürholz:** Conceptualization, Writing – review & editing. **Markus Neumayer:** Conceptualization, Writing – review & editing. **Hannes Wegleiter:** Conceptualization, Writing – review & editing, Supervision, Project administration, Funding acquisition.

Declaration of competing interest

The authors declare that they have no known competing financial interests or personal relationships that could have appeared to influence the work reported in this paper.

Data availability

Data will be made available on request.

Acknowledgments

The financial support by the Austrian Federal Ministry for Digital and Economic Affairs, the National Foundation for Research, Technology and Development, Austria, and the Christian Doppler Research Association, Austria are gratefully acknowledged.

Supported by TU Graz Open Access Publishing Fund, Austria.

Appendix A. Uncertainty for sum of values

Given M values x_i ($i = 1...M$) with associated uncertainty u_i and calculating their sum X

$$X = \sum_{i=1}^{M} x_i \tag{A.1}$$

then the corresponding uncertainty u for the sum X can be calculated as

$$u^2 = \sum_{i=1}^{M}\left(\frac{\partial X}{\partial x_i}\cdot u_i\right)^2 = \sum_{i=1}^{M} u_i^2 \tag{A.2}$$

[5] Unfortunately, there is no general value for when a device can be considered 'precise'. However, according to the authors, an uncertainty of 1/1000 may well be considered a good value for this type of measurements.

Table 2
Summary of uncertainties ($u_{variable}$, u_{const}, u_{total}) and listing of the relative contributions to $u_{variable}$ and u_{const} for the individual data analysis methods. Significant contributions, i.e. greater than ten percent, have been marked in color.

			Capacity	Capacity change	Coulombic efficiency	Internal resistance	DCA/DVA	ΔDCA/ΔDVA
$u_{variable}$		ppm	7.8	11	1	27	147–431	10–750
	$s_{td,t} \cdot T$	%	<1	<1	<1	<1	<1	<1
	$s_{td,I} \cdot T$	%	<1	<1	<1	<1	<1	<1
	$s_{td,V} \cdot T$	%	<1	<1	<1	<1	<1	33
	$s_{\vartheta,t} \cdot u_{\vartheta}$	%	<1	<1	<1	<1	<1	<1
	$s_{\vartheta,I} \cdot u_{\vartheta}$	%	<1	<1	<1	<1	<1	<1
	$s_{\vartheta,V} \cdot u_{\vartheta}$	%	<1	<1	<1	<1	3	2
	$u_{n,t}$	%	<1	<1	<1	<1	<1	<1
	$u_{n,I}$	%	<1	<1	2	<1	<1	<1
	$u_{n,V}$	%	<1	<1	<1	<1	97	65
	$u_{Vhigh,\vartheta}$	%	99	99	–	–	–	–
	$u_{Vlow,\vartheta}$	%	1	1	98	17	–	–
	u_{cutout}	%	–	–	–	83	–	–
u_{const}		ppm	700	0	≈ 0	700	700	1000
	$u_{c,t}$	%	<1	–	–	<1	<1	<1
	$u_{c,I}$	%	>99	–	–	>99	>99	>99
	$u_{c,V}$	%	<1	–	–	<1	<1	<1
	$s_{td,t} \cdot T_c$	%	<1	–	–	<1	<1	<1
	$s_{td,I} \cdot T_c$	%	<1	–	–	<1	<1	<1
	$s_{td,V} \cdot T_c$	%	<1	–	–	<1	<1	<1
u_{total}		ppm	700	11	1	701	715–822	1000–1250

Case 1. If u_i is constant u_{const}, then this can be evaluated as

$$u^2 = u_{const}^2 \cdot \sum_{i=1}^{M} 1 = M \cdot u_{const}^2 \tag{A.3}$$

Case 2. If u_i depends linearly on time t

$$t = i \cdot \Delta T \tag{A.4}$$

$$u_i = k \cdot t = k \cdot i \cdot \Delta T \tag{A.5}$$

with sample time ΔT and scaling factor k, then Eq. (A.2) can be evaluated as

$$u^2 = k^2 \cdot \Delta T^2 \cdot \sum_{i=1}^{M} i^2 \tag{A.6}$$

with

$$\sum_{i=1}^{M} i^2 = \frac{M(M+1)(2M+1)}{6} \tag{A.7}$$

and the assumption, that $M \gg 1$ this leads to

$$\sum_{i=1}^{M} i^2 \approx \frac{M(M)(2M)}{6} = \frac{M^3}{3} \tag{A.8}$$

and

$$u^2 = k^2 \cdot \Delta T^2 \cdot \frac{M^3}{3} \tag{A.9}$$

Since the total time T is equal to

$$T = M \cdot \Delta T \tag{A.10}$$

Eq. (A.9) can also be written as

$$u^2 = \frac{k^2 \cdot T^3}{3 \cdot \Delta T} \tag{A.11}$$

Application. Eq. (30) is used as example. The uncertainty for the time T, which is the sum of M time slots of length ΔT, each with associated uncertainty $u_{timeslot}(t)$

$$u_{timeslot}(t) = \sqrt{(s_{td,t} \cdot t \cdot \Delta T)^2 + (s_{\vartheta,t} \cdot u_{\vartheta chamber} \cdot \Delta T)^2 + u_{n,t}^2} \tag{A.12}$$

shall be calculated. The first term in Eq. (A.12) corresponds to 'Case 2' with k equal to

$$k = s_{td,t} \cdot \Delta T \tag{A.13}$$

From Eq. (A.11) then follows

$$u_{term1}^2 = \frac{s_{td,t}^2 \cdot \Delta T^2 \cdot T^3}{3 \cdot \Delta T} = s_{td,t}^2 \cdot \Delta T \cdot \frac{T^3}{3} \tag{A.14}$$

The second and third term correspond to 'Case 1'. As can be seen from Eq. (A.3) just a scaling by M is necessary. Overall this leads to an uncertainty for the sum u_{sum} of

$$u_{sum} = \sqrt{s_{td,t}^2 \cdot \Delta T \cdot \frac{T^3}{3} + M \cdot (s_{\vartheta,t} \cdot u_{\vartheta chamber} \cdot \Delta T)^2 + M \cdot u_{n,t}^2} \tag{A.15}$$

Appendix B. Uncertainty for mean of values

Given M values x_i ($i = 1...M$) with associated uncertainty u_i and calculating their mean $\bar{x}$

$$\bar{x} = \frac{1}{M} \cdot \sum_{i=1}^{M} x_i \tag{B.1}$$

then the corresponding uncertainty u for the mean $\bar{x}$ can be calculated as

$$u^2 = \sum_{i=1}^{M} \left(\frac{\partial X}{\partial x_i} \cdot u_i \right)^2 = \sum_{i=1}^{M} \left(\frac{u_i}{M} \right)^2 \tag{B.2}$$

Case 1. If u_i is constant u_{const}, then this can be evaluated as

$$u^2 = \left(\frac{u_{const}}{M} \right)^2 \cdot \sum_{i=1}^{M} 1 = \frac{u_{const}^2}{M} \tag{B.3}$$

Case 2. If u_i depends linearly on time t as shown in Eqs. (A.4) and (A.5), then Eq. (B.2) can be evaluated as

$$u^2 = \left(\frac{k \cdot \Delta T}{M} \right)^2 \cdot \sum_{i=1}^{M} i^2 \tag{B.4}$$

Then substituting the last term with the solution from Eq. (A.8) gives

$$u^2 = k^2 \cdot \Delta T^2 \cdot \frac{M}{3} \tag{B.5}$$

Finally, by substituting ΔT with T/M from Eq. (A.10) this leads to

$$u^2 = \frac{k^2 \cdot T^2}{3 \cdot M} \tag{B.6}$$

Application. Eq. (36) is used as example. The uncertainty for the average of the current I, with associated uncertainty $u_{\mathrm{var,I}}(t)$

$$u_{\mathrm{var,I}}(t) = \sqrt{(s_{\mathrm{td,I}} \cdot t \cdot I)^2 + (s_{\vartheta,\mathrm{I}} \cdot u_{\vartheta\mathrm{shuntAndRef}} \cdot I)^2 + u_{\mathrm{n,I}}^2} \tag{B.7}$$

shall be calculated. The first term in Eq. (B.7) corresponds to 'Case 2' with k equal to

$$k = s_{\mathrm{td,I}} \cdot I \tag{B.8}$$

From Eq. (B.6) then follows

$$u_{\mathrm{term1}}^2 = \frac{s_{\mathrm{td,I}}^2 \cdot I^2 \cdot T^2}{3 \cdot M} \tag{B.9}$$

The second and third term correspond to 'Case 1'. As can be seen from Eq. (B.3) just a simple scaling is necessary. Overall this leads to an uncertainty for the average u_{average} of

$$u_{\mathrm{average}} = \sqrt{\frac{s_{\mathrm{td,I}}^2 \cdot I^2 \cdot T^2}{3 \cdot M} + \frac{(s_{\vartheta,\mathrm{I}} \cdot u_{\vartheta\mathrm{shuntAndRef}} \cdot I)^2}{M} + \frac{u_{\mathrm{n,I}}^2}{M}} \tag{B.10}$$

References

[1] V. Ruiz, F.D. Persio, Standards for the performance and durability assessment of electric vehicle batteries, Technical Report, Joint Research Centre (European Commission), 2018.

[2] J.P. Christophersen, Battery Technology Life Verification Test Manual Revision 1, Technical Report, U.S. Department of Energy, Office of Scientific and Technical Information (OSTI), 2012, http://dx.doi.org/10.2172/1064046.

[3] D. Heeger, M. Partridge, V. Trullinger, D. Wesolowski, Lithium Battery Health and Capacity Estimation Techniques Using Embedded Electronics, Technical Report, U.S. Department of Energy, Office of Scientific and Technical Information (OSTI), 2017, http://dx.doi.org/10.2172/1596204.

[4] J.C. Burns, A. Kassam, N.N. Sinha, L.E. Downie, L. Solnickova, B.M. Way, J.R. Dahn, Predicting and extending the lifetime of Li-ion batteries, J. Electrochem. Soc. 160 (9) (2013) A1451–A1456, http://dx.doi.org/10.1149/2.060309jes.

[5] F. Yang, D. Wang, Y. Zhao, K.-L. Tsui, S.J. Bae, A study of the relationship between coulombic efficiency and capacity degradation of commercial lithium-ion batteries, Energy 145 (2018) 486–495, http://dx.doi.org/10.1016/j.energy.2017.12.144.

[6] B. Gyenes, D.A. Stevens, V.L. Chevrier, J.R. Dahn, Understanding anomalous behavior in Coulombic efficiency measurements on Li-ion batteries, J. Electrochem. Soc. 162 (3) (2014) A278–A283, http://dx.doi.org/10.1149/2.0191503jes.

[7] A.J. Smith, J.C. Burns, S. Trussler, J.R. Dahn, Precision measurements of the Coulombic efficiency of lithium-ion batteries and of electrode materials for lithium-ion batteries, J. Electrochem. Soc. 157 (2) (2010) A196, http://dx.doi.org/10.1149/1.3268129.

[8] A.J. Smith, J.C. Burns, J.R. Dahn, A high precision study of the Coulombic efficiency of Li-ion batteries, Electrochem. Solid-State Lett. 13 (12) (2010) A177, http://dx.doi.org/10.1149/1.3487637.

[9] T.M. Bond, J.C. Burns, D.A. Stevens, H.M. Dahn, J.R. Dahn, Improving precision and accuracy in Coulombic efficiency measurements of Li-ion batteries, J. Electrochem. Soc. 160 (3) (2013) A521–A527, http://dx.doi.org/10.1149/2.014304jes.

[10] J. Xia, L. Ma, J. Dahn, Improving the long-term cycling performance of lithium-ion batteries at elevated temperature with electrolyte additives, J. Power Sources 287 (2015) 377–385, http://dx.doi.org/10.1016/j.jpowsour.2015.04.070.

[11] J.C. Burns, G. Jain, A.J. Smith, K.W. Eberman, E. Scott, J.P. Gardner, J.R. Dahn, Evaluation of effects of additives in wound Li-ion cells through high precision coulometry, J. Electrochem. Soc. 158 (3) (2011) A255, http://dx.doi.org/10.1149/1.3531997.

[12] A.J. Smith, J.C. Burns, D. Xiong, J.R. Dahn, Interpreting high precision coulometry results on Li-ion cells, J. Electrochem. Soc. 158 (10) (2011) A1136–A1142, http://dx.doi.org/10.1149/1.3625232.

[13] D. Linden, T.B. Reddy, Lindens Handbook of Batteries, The McGraw-Hill Companies, Inc., 2011.

[14] B. Schweighofer, H. Wegleiter, M. Recheis, P. Fulmek, Fast and accurate battery model applicable for EV and HEV simulation, in: 2012 IEEE International Instrumentation and Measurement Technology Conference Proceedings, IEEE, 2012, pp. 565–570, http://dx.doi.org/10.1109/i2mtc.2012.6229525.

[15] B. Schweighofer, M. Recheis, T. Gallien, H. Wegleiter, Fast and accurate battery model including temperature dependency, in: IECON 2013 - 39th Annual Conference of the IEEE Industrial Electronics Society, IEEE, 2013, pp. 6740–6745, http://dx.doi.org/10.1109/iecon.2013.6700248.

[16] J. Wang, Y. Jia, N. Yang, Y. Lu, M. Shi, X. Ren, D. Lu, Precise equivalent circuit model for Li-ion battery by experimental improvement and parameter optimization, J. Energy Storage 52 (2022) 104980, http://dx.doi.org/10.1016/j.est.2022.104980.

[17] V.J. Ovejas, A. Cuadras, Effects of cycling on lithium-ion battery hysteresis and overvoltage, Sci. Rep. 9 (1) (2019) http://dx.doi.org/10.1038/s41598-019-51474-5.

[18] A.J. Smith, J.R. Dahn, Delta differential capacity analysis, J. Electrochem. Soc. 159 (3) (2012) A290–A293, http://dx.doi.org/10.1149/2.076203jes.

[19] M. Dubarry, C. Truchot, B.Y. Liaw, Cell degradation in commercial LiFePO4 cells with high-power and high-energy designs, J. Power Sources 258 (2014) 408–419, http://dx.doi.org/10.1016/j.jpowsour.2014.02.052.

[20] L. Wang, X. Zhao, L. Liu, C. Pan, State of health estimation of battery modules via differential voltage analysis with local data symmetry method, Electrochim. Acta 256 (2017) 81–89, http://dx.doi.org/10.1016/j.electacta.2017.10.025.

[21] H.M. Dahn, A.J. Smith, J.C. Burns, D.A. Stevens, J.R. Dahn, User-friendly differential voltage analysis freeware for the analysis of degradation mechanisms in Li-ion batteries, J. Electrochem. Soc. 159 (9) (2012) A1405–A1409, http://dx.doi.org/10.1149/2.013209jes.

[22] JCGM, Evaluation of measurement data - Guide to the expression of uncertainty in measurement, first ed., Joint Committee for Guides in Metrology, 2008.

[23] A.G. González, M.Á. Herrador, A.G. Asuero, J. Martín, A practical way to ISO/GUM measurement uncertainty for analytical assays including in-house validation data, in: Quality Control in Laboratory, InTech, 2018, pp. 109–148, http://dx.doi.org/10.5772/intechopen.72048.

[24] A. Farmann, D.U. Sauer, A study on the dependency of the open-circuit voltage on temperature and actual aging state of lithium-ion batteries, J. Power Sources 347 (2017) 1–13, http://dx.doi.org/10.1016/j.jpowsour.2017.01.098.